Inorg. Chem. **2007**, *46*, 3217−3230

From Chain to Network: Design and Analysis of Novel Organic−Inorganic Assemblies from Organically Functionalized Zinc-Substituted Polyoxovanadates and Zinc Organoamine Subunits

Yanfei Qi, Yangguang Li, Chao Qin, Enbo Wang,* Hua Jin, Dongrong Xiao, Xinglong Wang, and Song Chang

Key Laboratory of Polyoxometalates Science of Ministry of Education, Department of Chemistry, Northeast Normal University, Ren Min Street No. 5268, Changchun, Jinlin 130024, People's Republic of China

Received December 7, 2006

A series of novel organic–inorganic assemblies, $[Zn(Meen)_2]_2[(4,4'\text{-bipy})Zn_2As_8V_{12}O_{40}(H_2O)]$ (**1**), $[Zn(en)_2(H_2O)][Zn(en)_2(4,4'\text{-bipy})Zn_2As_8V_{12}O_{40}(H_2O)]\cdot 3H_2O$ (**2**), $[\{Zn(en)_3\}_2\{Zn_2As_8V_{12}O_{40}(H_2O)\}]\cdot 4H_2O\cdot 0.25bipy$ (**3**) and $[Zn_2(en)_5]\{[Zn(en)_2][(bpe)HZn_2As_8V_{12}O_{40}(H_2O)]_2\}\cdot 7H_2O$ (**4**) [en = ethylenediamine, Meen = 1,2-diaminopropane, 4,4′-bipy = 4,4′-bipyridine, and bpe = 1,2-bis(4-pyridyl)ethane] constructed from organically modified Zn-substituted polyoxovanadates and zinc organoamine subunits have been synthesized. Each anion cluster of compound **1** is directly linked by the 4,4′-bipy ligand into a one-dimensional (1D) straight chain. The secondary metal complex $[Zn(Meen)_2]^{2+}$ acts as an isolated countercation. The 1D chain structure of **2** is similar to that of **1** but sinuate because of the secondary metal complex $[Zn(en)_2]^{2+}$ decorated on the anion cluster. The en ligands covalently bonding to the surface anion of **3** not only support the secondary metal complex $[Zn(en)_2]^{2+}$ but also coordinate to another anion through the secondary metal complex $[Zn(en)_2]^{2+}$ bridge to form an "eight-shaped" chiral helix. The unprecedented 2D layer of compound **4** with large nanosized inner rectangular cavities [33.669(6) ×14.720(8) Å] is successfully achieved through the anion clusters polymerized first into chains by flexible organic ligands and then secondary metal complexes bridged between the chains. The different coordination abilities and geometries of the bidentate organodiamine ligands used in the four-reaction systems play important roles in the formation of the final structures: from straight chains to sinuate chains, to helical chiral chains, and finally to a 2D layer with helices.

Introduction

The design and construction of porous solids from performed metal clusters have attracted much attention because of interest in the creation of nanometer-sized spaces and their potential applications in gas storage, ion exchange, or heterogeneous catalysis.[1] For example, Yaghi and co-workers utilized metal carboxylate clusters as vertices to construct metal−organic frameworks with large channels for gas storage.[2] Férey et al. created a mesoporous zeotype cubic architecture, by scaling up the size of the building units, that has potential as a nanomold for monodisperse nanomaterials.[3] In recent years, polyoxometalates (POMs),[4] as a unique class of metal oxide clusters with enormous structural variety and electronic properties leading to potential applications[5] in catalysis, biology, magnetism, nonlinear optics, and medicine, are extremely versatile inorganic building blocks and have

* To whom correspondence should be addressed. E-mail: wangenbo@pubilc.cc.jl.cn and wangeb889@nenu.edu.cn.

(1) (a) Cheetham, A. K.; Férey, G.; Loiseau, T. *Angew. Chem., Int. Ed.* **1999**, *38*, 3268−3292. (b) Hagrman, P. J.; Hagrman, D.; Zubieta, J. *Angew. Chem., Int. Ed.* **1999**, *38*, 2638−2684. (c) Tripathi, A.; Hughbanks, T.; Clearfield, A. *J. Am. Chem. Soc.* **2003**, *125*, 10528−15029. (d) Zhang, M. B.; Zhang, J.; Zheng, S. T.; Yang, G. Y. *Angew. Chem., Int. Ed.* **2005**, *44*, 1385−1388.

(2) (a) Rosi, N. L.; Eckert, J.; Eddaoudi, M.; Vodak, D. T.; Kim, J.; O'Keeffe, M.; Yaghi, O. M. *Science* **2003**, *300*, 1127−1129. (b) Eddaoudi, M.; Moler, D. B.; Li, H.; Chen, B. L.; Reineke, T. M.; O'Keeffe, M.; Yaghi, O. M. *Acc. Chem. Res.* **2001**, *34*, 319−330. (c) Li, H.; Eddaoudi, M.; O'Keeffe, M.; Yaghi, O. M. *Nature* **1999**, *402*, 276−279. (d) Chen, B.; Eddaoudi, M.; Reineke, T. M.; Kampf, J. W.; O'Keeffe, M.; Yaghi, O. M. *J. Am. Chem. Soc.* **2000**, *122*, 11559−11560.

(3) (a) Férey, G.; Mellot-Draznieks, C.; Serre, C.; Millange, F.; Dutour, J.; Surblé, S.; Margiolaki, I. *Science* **2005**, *309*, 2040−2042. (b) Férey, G. *Science* **2001**, *291*, 994−995. (c) Férey, G. *J. Solid State Chem.* **2000**, *152*, 37−48.

10.1021/ic062338l CCC: $37.00
Published on Web 03/20/2007

been extensively introduced in the construction of functional porous materials.[6] However, despite their practical importance and relatively developed synthetic chemistry, the biggest challenge in the field continues to be to achieve the "design" of hybrid porous solids. In general, there are two principal methods to synthesize porous POM-based materials, especially covalently bonded extended structures: (1) Formation from a functionalized POM backbone; that is, the organic polymers contain covalently bonded POMs in their backbone or as pendant groups.[7] For example, one or several terminal O atoms of $[Mo_6O_{19}]^{2-}$ can be replaced by various organic species, including the nitrosyl, diazenido, hydrazido, organmetallic, diazoalkyl, and imido ligands.[8] These organic-functionalized $[Mo_6O_{19}]^{2-}$ groups can be further used to generate main-chain POM-containing polymers.[9] POMs as side-chain pendants have been grafted to a number of polymers,[7,10,11] such as macroporous silica materials functionalized with POMs.[11] The approach to modifying the surface of these clusters through covalently bonded organic species may provide a rational way to not only fine-tune the material properties but also bring about novel synergistic effects between inorganic clusters and organic segments.[12] However, this approach has not been extensively explored. (2) Formation from POMs decorated by secondary transition-metal complexes (TMCs) linked through bridging O groups. POMs coordinate to secondary metal centers of the polymer to achieve one-, two-, or three-dimensional (1D, 2D, or 3D) coordination polymers.[13] The various well-characterized structures of definite nanoscopic sizes of POMs could be used as spacers to control the sizes of the cavities. To date, the majority of POM-based polymers have been successfully synthesized by this approach.[14,15] Recently, Zubieta and co-workers employed diphosphonate ligands, oxomolybdenum, and metal organoimine to fashion new solid-state architectures that exhibit composite or new physicochemical properties.[14e,f]

Chart 1. Synthesis Strategies for Porous Materials

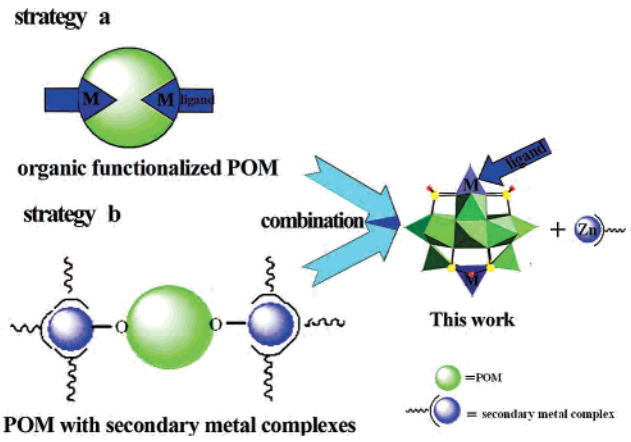

Our approach, similar to Zubieta's, consists of the conflation of these two general strategies, i.e., organically functionalized POMs first form main-chain POM-containing polymers that are further decorated by secondary metal complexes (Chart 1). Among the many different types of POMs, despite the transition-metal (TM)-substituted POMs have receiving much attention for their catalytic properties in organic oxidation, attempts to link these TM-substituted POMs in order to construct extended solid frameworks have been rarely studied. In fact, replacement of the metal centers (Mo, V, and W) of the POM backbones with other transition metals (Fe, Co, Ni, Cu, and Zn) could increase the surface charge density and improve the coordination capability of the surface O atoms. In addition, these active TM positions are more easily coordinated with various N- or O-containing organic functionalities, which make it possible to construct main-chain POM-based backbone structures. During our

(4) (a) Pope, M. T. *Heteropoly and Isopoly Oxometalates*; Springer: Berlin, 1983. (b) Pope, M. T.; Müller, A. *Angew. Chem., Int. Ed. Engl.* **1991**, *30*, 34−48. (c) Hill, C. L. *Chem. Rev.* **1998**, *98*, 327−357. (d) Fukaya, K.; Yamase, T. *Angew. Chem., Int. Ed.* **2003**, *42*, 654−658. (e) Wu, C. D.; Lu, C. Z.; Zhuang, H. H.; Huang, J. S. *J. Am. Chem. Soc.* **2002**, *124*, 3836−3837.

(5) (a) Müller, A.; Shah, S. Q. N.; Bögge, H.; Schmidtmann, M. *Nature* **1999**, *397*, 48−50. (b) Chui, S. S. Y.; Lo, S. M. F.; Charmant, J. P. H.; Orpen, A. G.; Williams, I. D. *Science* **1999**, *283*, 1148−1150. (c) Coronado, E.; Gómez-Garcýá, C. J. *Chem. Rev.* **1998**, *98*, 273−296. (d) Yamase, T. *Chem. Rev.* **1998**, *98*, 307−326. (e) Kang, J.; Nelson, J. A.; Lu, M.; Xie, B. H.; Peng, Z. H.; Powell, D. R. *Inorg. Chem.* **2004**, *43*, 6408−6413. (f) Pope, M. T. *Prog. Inorg. Chem.* **1991**, *30*, 181−257.

(6) (a) Chesnut, D. J.; Hagrman, D.; Zapf, P. J.; Hammond, R. P.; LaDuca, R.; Haushalter, R. C.; Zubieta, J. *Coord. Chem. Rev.* **1999**, 190−192, 737−769. (b) Khan, M. I.; Yohannes, E.; Powell, D. *J. Chem. Soc., Chem. Commun.* **1999**, *1*, 23−24. (c) Khan, M. I.; Yohannes, E.; Doedens, R. J. *Angew. Chem., Int. Ed.* **1999**, *38*, 1292−1294. (d) Do, J.; Bontchev, R. P.; Jacobson, A. J. *Inorg. Chem.* **2000**, *39*, 4305−4310.

(7) (a) Judeinstein, P. *Chem. Mater.* **1992**, *4*, 4−7. (b) Moore, A. R.; Kwen, H.; Beatty A. M.; Maatta, E. A. *Chem. Commun.* **2000**, 1793−1794.

(8) (a) Gouzerh, P.; Jeannin, Y.; Proust, A.; Robert, F. *Angew. Chem., Int. Ed. Engl.* **1989**, *28*, 1363−1364. (b) Proust, A.; Thouvenot, R.; Robert, F.; Gouzerh, P. *Inorg. Chem.* **1993**, *32*, 5299−5303. (c) Bank, S.; Liu, S.; Shaikh, S. N.; Sun, X.; Zubieta, J.; Ellis, P. D. *Inorg. Chem.* **1988**, *27*, 3535−3543. (d) Du, Y.; Rheingold, A. L.; Maatta, E. A. *J. Am. Chem. Soc.* **1992**, *114*, 346−348. (e) Strong, J. B.; Yap, G. P. A.; Ostrander, R.; Liable-Sands, L. M.; Rheingold, A. L.; Thouvenot, R.; Gouzerh, P.; Maatta, E. A. *J. Am. Chem. Soc.* **2000**, *122*, 639−649. (f) Wei, Y.; Xu, B.; Barnes, C. L.; Peng, Z. *J. Am. Chem. Soc.* 2001, *123*, 4083−4084. (g) Clegg, W.; Errington, R. J.; Fraser, K.; Holmes, S. A.; Schäfer, A. *J. Chem. Soc., Chem. Commun.* **1995**, 455−456.

(9) Xu, L.; Lu, M.; Xu, B.; Wei, Y.; Peng, Z.; Powell, D. R. *Angew. Chem., Int. Ed.* **2002**, *41*, 4129−4132.

(10) (a) Mayer, C. R.; Cabuil, V.; Lalot, T.; Thouvenot, R. *Angew. Chem., Int. Ed.* **1999**, *38*, 3672−3675. (b) Mayer, C. R.; Thouvenot, R.; Lalot, T. *Chem. Mater.* **2000**, *2*, 257−260.

(11) (a) Schroden, R. C.; Blanford, C. F.; Melde, B. J.; Johnson, B. J. S.; Stein, A. *Chem. Mater.* **2001**, *13*, 1074−1081. (b) Johnson, B. J. S.; Stein, A. *Inorg. Chem.* **2001**, *40*, 801−808.

(12) (a) Gouzerh, P.; Proust, A. *Chem. Rev.* **1998**, *98*, 77−112. (b) Zeng, H.; Newkome, G. R.; Hill, C. L. *Angew. Chem., Int. Ed.* **2000**, *39*, 1772−1774.

(13) Hagrman, D.; Rose, C. D. J.; Zubieta, J.; Haushalter, R. C. *Angew. Chem., Int. Ed. Engl.* **1997**, *36*, 873−876.

(14) (a) Zapf, P. J.; Warren, C. J.; Haushalter, R. C.; Zubieta, J. *Chem. Commun.* **1997**, 1543−1544. (b) Hagrman, P. J.; Hagrman, D.; Zubieta, J. *Inorg. Chem.* **2000**, *39*, 3252−3260. (c) LaDuuca, R. L., Jr.; Rarig, R. S., Jr.; Zubieta, J. *Inorg. Chem.* **2001**, *40*, 607−612. (d) Finn, R. C.; Rarig, R. S., Jr.; Zubieta, J. *Inorg. Chem.* **2002**, *41*, 2109−2123. (e) Burkholder, E.; Golub, V.; O'Connor, C. J.; Zubieta, J. *Inorg. Chem.* **2004**, *43*, 7014−7029. (f) Gabriel Armatas, N.; Burkholder, E.; Zubieta, J. *J. Solid State Chem.* **2005**, *178*, 2430−2435.

(15) (a) Zhang, X. M.; Tong, M. L.; Chen, X. M. *Chem. Commun.* **2000**, 1817−1818. (b) Liu, C. M.; Gao, S.; Kou, H. Z. *Chem. Commun.* **2001**, 1670−1671. (c) Lu, C. Z.; Wu, C. D.; Lu, S. F.; Liu, J. C.; Wu, Q. J.; Zhuang, H. H.; Huang, J. S. *Chem. Commun.* **2002**, 152−153. (d) Lin, B. Z.; Liu, S. X. *Chem. Commun.* **2002**, 2126−2127. (e) Dai, Z. M.; Shi, Z.; Li, G. H.; Zhang, D.; Fu, W. S.; Jin, H. Y.; Feng, S. H. *Inorg. Chem.* **2003**, *42*, 7396−7402.

Table 1. Crystal Data and Structure Refinements for Compounds **1**−**4**

complex	**1**	**2**	**3**	**4**
formula	$C_{22}H_{54}As_8N_{10}O_{41}V_{12}Zn_4$	$C_{18}H_{50}As_8N_{10}O_{45}V_{12}Zn_4$	$C_{29}H_{120}As_{16}N_{25}O_{90}V_{24}Zn_8$	$C_{76}H_{200}As_{32}N_{36}O_{178}V_{48}Zn_{14}$
fw	2586.84	2598.80	5203.72	10224.49
cryst syst	monoclinic	monoclinic	monoclinic	monoclinic
space group	*C*2/*c*	*P*2(1)/*n*	*P*2(1)/*n*	*P*2(1)/*n*
a (Å)	16.420(3)	15.037(3)	19.665(4)	12.901(3)
b (Å)	18.624(4)	15.974(3)	28.701(6)	22.591(5)
c (Å)	26.339(5)	31.224(6)	27.002(5)	25.299(5)
α (deg)	90	90	90	90
β (deg)	100.08(3)	101.16(3)	93.87(3)	103.56(3)
γ (deg)	90	90	90	90
V (Å^3)	7930(3)	7358(3)	15205(5)	7168(2)
Z, D_c (Mg/m^3)	4, 2.163	4, 2.346	4, 2.272	4, 2.370
μ (mm^{-1})	5.922	6.387	6.183	6.392
reflns collcd/ unique	29 247/6901 [R_{int} = 0.0901]	53 010/12 873 [R_{int} = 0.0808]	114 816/26 677 [R_{int} = 0.1237]	36 008/12 627 [R_{int} = 0.0374]
F(000)	4960	4992	10028	2384
GOF on F^2	1.240	1.029	1.048	1.060
R1[a] [$I > 2\sigma(I)$]	0.0788	0.0733	0.0714	0.0475
wR2[b]	0.2193	0.1964	0.1637	0.1610
largest diff peak, hole (e Å^{-3})	2.746, −2.001	3.495, −1.619	1.716, −1.522	2.515, −1.303

effort to construct these materials, the unique $[Zn_2As_8V_{12}O_{40}]^{4-}$ building block[16] captured our attention for the following reasons: (a) It is a contrapuntal Zn_2-substituted POM that can be directly linked by linear organoamine ligands in two opposite directions. This offers an opportunity to prepare new complexes containing inorganic POM backbones coordinated directly by organic functionalities. (b) The steric orientations of the coordination sites are considerably flexible, which will cause the V═O groups to connect secondary transition-metal ions in different directions. (c) The As^{III} atoms with the electron lone pairs capping on the $[Zn_2As_8V_{12}O_{40}]^{4-}$ cluster can block the coordination sites that are not required and thus leave specific sites free for transition-metal connectors. Hence, the selection of such POM anions can further guide the self-assembly reaction.

To implement the above idea, considering the important influence of the organic ligands on the structures of the POM-based polymers, the different rigid and/or flexible N-donor ligands [4,4′-bipyridine (4,4′-bipy), 1,2-bis(4-pyridyl)ethane (bpe), ethylenediamine (en), and 1,2-diaminopropane (Meen)] were used for our synthetic strategy. In addition, involvement of more than one type of organic molecule with distinctive linking manners and coordination preferences into the inorganic substructures could increase the complexity of the hierarchical structures and fine-tune the materials' properties. Others[17] and we[18] demonstrate in recent contributions that this method produces a series of novel materials.

On the basis of the aforementioned points, herein we systematically elucidate the parameters that control the assembly of these TM-substituted POM clusters into specific architectures and report the synthesis and characterization of the following new system: $[Zn(Meen)_2]_2[(4,4'\text{-bipy})Zn_2As_8V_{12}O_{40}(H_2O)]$ (**1**), $[Zn(en)_2(H_2O)][Zn(en)_2(4,4'\text{-bipy})Zn_2As_8V_{12}O_{40}(H_2O)]\cdot 3H_2O$ (**2**), $[\{Zn(en)_3\}_2Zn_2As_8V_{14}O_{40}(H_2O)]\cdot 4H_2O\cdot 0.25bpy$ (**3**), and $[Zn_2(en)_5]\{[Zn(en)_2][(bpe)HZn_2As_8V_{12}O_{40}(H_2O)]_2\}\cdot 7H_2O$ (**4**). Furthermore, the electrochemical properties of these compounds have been studied by using bulk-modified carbon paste electrodes (CPEs). The magnetic studies of **1** and **4** show antiferromagnetic interactions within the V^{IV} pairs.

Experimental Section

Materials and Methods. All chemicals were commercially purchased and used without further purification. Elemental analyses (C, H, and N) were performed on a Perkin-Elmer 2400 CHN elemental analyzer. Zn, As, and V were determined by a Leaman inductively coupled plasma spectrometer. IR spectra were recorded in the range 400−4000 cm^{-1} on an Alpha Centaurt Fourier transform (FT)-IR spectrophotometer using KBr pellets. Thermogravimetric analyses (TGA) were performed on a Perkin-Elmer TGA7 instrument in flowing N_2 with a heating rate of 10 °C min^{-1}. A CHI 660 Electrochemical Workstation connected to a Digital-586 personal computer was used for control of the electrochemical measurements and for data collection. A conventional three-electrode system was used. The working electrodes were compounds **1**−**4** bulk-modified CPEs. A saturated calomel electrode (SCE) was used as the reference electrode and Pt gauze as a counter electrode. The working electrodes were prepared following our earlier method. The magnetic susceptibility data were measured with the use of a Quantum Design SQUID MPMS-XL magnetometer.

Synthesis of $[Zn(Meen)_2]_2[(4,4'\text{-bipy})Zn_2As_8V_{12}O_{40}(H_2O)]$ (1). A mixture of NH_4VO_3 (1 mmol), As_2O_3 (0.5 mmol), $ZnCl_2\cdot 7H_2O$ (0.27 mmol), 4,4′-bipy (0.8 mmol), Meen (0.8 mL), and HNO_3 (0.1 mL, 16 M) was dissolved in distilled water (6 mL). Then the solution was sealed in a 15-mL Teflon-lined bomb at 170 °C for 5 days and resulted in brown block crystals of **1** (yield: ca. 59.8% based on V). Anal. Calcd for $C_{22}H_{54}As_8N_{10}O_{41}V_{12}Zn_4$: C, 10.21; H, 2.10; N, 5.41; V, 23.63; As, 23.17; Zn, 10.11. Found: C, 10.27; H, 2.21; N, 5.32; V, 23.56; As, 23.19; Zn, 10.19. IR (KBr pellet, cm^{-1}): 3457 (w), 3317 (w), 3251 (s), 2960 (w), 2917 (w), 1609 (s), 1588 (m), 1460 (w), 1418 (w), 1381 (w), 1227 (w), 1067 (w), 988 (s), 823 (m), 717 (s), 636 (m), 540 (w), 503 (w), 461 (m).

(16) Zheng, S. T.; Zhang, J.; Xu, J. Q.; Yang, G. Y. *Eur. J. Inorg. Chem.* **2004**, 2004−2007.
(17) (a) Tao, J.; Zhang, X. M.; Tong, M. L.; Chen, X. M. *J. Chem. Soc., Dalton Trans.* **2001**, 770−771. (b) Lu, C. Z.; Wu, C. D.; Zhuang, H. H.; Huang, J. S. *Chem. Mater.* **2002**, *14*, 2649−2651. (c) Liu, C. M.; Zhang, D. Q.; Xiong, M.; Zhu, D. B. *Chem. Commun.* **2002**, 1416−1417. (d) Lisnard, L.; Dolbecq, A.; Mialane, P.; Marrot, J.; Codjovi, E.; Sécheresse, F. *J. Chem. Soc., Dalton Trans.* **2005**, 3919−3922.
(18) (a) Lü, J.; Shen, E. H.; Yuan, M.; Li, Y. G.; Wang, E. B.; Hu, C. W.; Xu, L.; Peng, J. *Inorg. Chem.* **2003**, *42*, 6956−6958. (b) Lü, J.; Li, Y. G.; Shen, E. H.; Yuan, M.; Wang, E. B.; Hu, C. W.; Xu, L. *J. Solid State Chem.* **2004**, *177*, 1771−1775.

Synthesis of $[Zn(en)_2(H_2O)][Zn(en)_2(4,4'\text{-bipy})Zn_2As_8V_{12}O_{40}(H_2O)]\cdot 3H_2O$ (2). A mixture of NH_4VO_3 (1 mmol), As_2O_3 (0.5 mmol), $ZnCl_2\cdot 7H_2O$ (0.27 mmol), 4,4′-bipy (0.8 mmol), en (0.3 mL), and HNO_3 (0.1 mL, 16 M) was dissolved in distilled water (6 mL). Then the solution was sealed in a 15-mL Teflon-lined bomb at 170 °C for 5 days and resulted in brown block crystals of **2** (yield: ca. 30.2% based on V). Anal. Calcd for $C_{18}H_{50}As_8N_{10}O_{45}V_{12}Zn_4$: C, 8.32; H, 1.94; N, 5.39; V, 23.52; As, 23.06; Zn, 10.06. Found: C, 8.27; H, 1.99; N, 5.34; V, 23.59; As, 23.09; Zn, 10.10. IR (KBr pellet, cm^{-1}): 3439 (m), 3323 (w), 3269 (s), 2939 (w), 1607 (s), 1583 (s), 1529 (w), 1461 (w), 1407 (w), 1326 (w), 1216 (w), 1072 (w), 984 (s), 822 (m), 717 (w), 673 (m), 641 (m), 551 (w), 508 (m), 445 (m).

Synthesis of $[\{Zn(en)_3\}_2Zn_2As_8V_{14}O_{40}(H_2O)]\cdot 4H_2O\cdot 0.25bpy$ (3). A mixture of NH_4VO_3 (1 mmol), As_2O_3 (0.5 mmol), $ZnCl_2\cdot 7H_2O$ (0.27 mmol), 4,4′-bipy (0.3 mmol), en (0.5 mL), and HNO_3 (0.1 mL, 16 M) was dissolved in distilled water (6 mL). Then the solution was sealed in a 15-mL Teflon-lined bomb at 170 °C for 5 days and resulted in brown block crystals of **3** (yield: ca. 39.4% based on V). Anal. Calcd for $C_{29}H_{120}As_{16}N_{25}O_{90}V_{24}Zn_8$: C, 6.69; H, 2.32; N, 6.73; As, 23.04; Zn, 10.05; V, 23.49. Found: C, 12.11; H, 1.38; N, 6.37; As, 21.38; Ni, 5.34; V, 25.38. IR (KBr pellet, cm^{-1}): 3434 (m), 3269 (s), 2944 (w), 2885 (w), 1591 (s), 1455 (w), 1279 (w), 1108 (w), 982 (s), 717 (s), 636 (m), 546 (w), 505 (w), 460 (m).

Synthesis of $[Zn_2(en)_5]\{[Zn(en)_2][(bpe)HZn_2As_8V_{12}O_{40}(H_2O)]_2\}\cdot 7H_2O$ (4). A mixture of NH_4VO_3 (1 mmol), As_2O_3 (0.5 mmol), $ZnCl_2\cdot 7H_2O$ (0.27 mmol), bpe (1 mmol), en (0.3 mL), and HNO_3 (0.1 mL, 16 M) was dissolved in distilled water (6 mL). Then the solution was sealed in a 15-mL Teflon-lined bomb at 170 °C for 5 days and resulted in brown block crystals of **4** (yield: ca. 36.6% based on V). Anal. Calcd for $C_{76}H_{200}As_{32}N_{36}O_{178}V_{48}Zn_{14}$: C, 8.93; H, 1.97; N, 4.93; As, 23.45; Zn, 8.95; V, 23.91. Found: C, 9.02; H, 1.94; N, 4.97; As, 23.48; Zn, 8.99; V, 23.87. IR spectrum (KBr pellet, cm^{-1}): 3447 (m), 3362 (w), 3266 (w), 2944 (w), 1616 (s), 1506 (w), 1459 (w), 1435 (w), 1369 (w), 1330 (w), 1280 (w), 1227 (w), 1104 (w), 986 (s), 823 (m), 716 (s), 667 (w), 640 (s), 547 (w), 504 (w), 462 (m).

X-ray Crystallography. The measurements for compounds **1**−**3** were performed on a Rigaku R-AXIS RAPID IP diffractometer, while the structure of **4** was collected on a Bruker SMART CCD diffractometer. In all cases, the data were collected at 293 K, and graphite-monochromated Mo Kα radiation ($\lambda = 0.710\ 73$ Å) was used. Empirical absorption corrections were applied for compounds **1**−**3**. An empirical absorption correction was applied for compound **4** utilizing the *SADABS* routine. The structures were solved by direct methods and refined by full-matrix least squares on F^2 using the *SHELXL-97* software.[19a,b] For **2**, in the cluster structure, two As atoms and two V atoms were disordered. The As2 and As3 atoms were all disordered over two positions (As2 with an occupancy of 0.75, As2A with 0.25, As3 with 0.85, and As3A with 0.25). The V2 and V3 atoms were disordered over two positions [V2 (3) with an occupancy of 0.70 and V2A (3A) with an occupancy of 0.30]. All of the non-H atoms were refined anisotropically except for the disordered N3, N4, N5, N6, C11, C12, C13, C14, C15, and C16 in **1**, N10 in **2**, and N21, N22, N23, N24, C21, C22, and C24 in **3**. The electron density found in **4** close to the V and As atoms are simply omitted for the heavy-atom effect. In each structure, H atoms of organic ligands were fixed in ideal positions. The H atoms attached to water were not located. The crystal data and structure refinements of compounds **1**−**4** were summarized in Table 1.

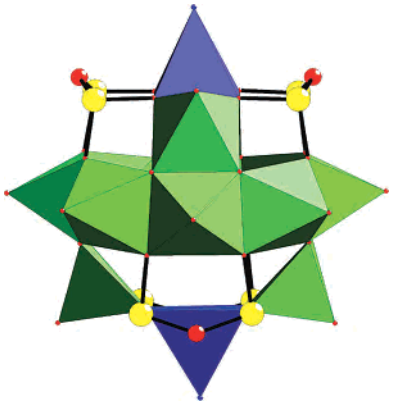

Figure 1. View of the basic building block $[Zn_2As_8V_{12}O_{40}(H_2O)]^{4-}$ cluster.

Results and Discussion

Structure Description. The Zn-substituted polyoxoanion backbones in compounds **1**−**3**, $[Zn_2As_8V_{12}O_{40}]^{4-}$, and **4**, $[HZn_2As_8V_{12}O_{40}]^{3-}$, are similar to the only one reported recently by Yang et al.,[16] which is built up from 2 $NZnO_4$ square pyramids, 12 VO_5 square pyramids, and 8 AsO_3 trigonal pyramids, with one neutral H_2O molecule at the center (Figure 1). The cluster can also be considered as two Zn^{2+} ions substituting for two VO^{2+} groups located between the As_2O_5 units of the well-known $[As_8V_{14}O_{42}(X)]^{n-}$ (X = H_2O, NO_3^-) anion. Two AsO_3 groups are joined together by an O bridge to form a As_2O_5 moiety. Eight VO_5 square pyramids are held together to form an eight-membered ring by edge-sharing O atoms. In addition, another four VO_5 square pyramids are divided into two groups; each group of VO_5 square pyramids share their edges with the $NZnO_4$ square pyramids to form a trimer. The two trimers are on opposite sides of the ring and are connected across the ring by sharing the edges with two VO_5 square pyramids, respectively. The remaining four faces are capped by the As_2O_5 units to give a ball-like structure. The V−O bond lengths range from 1.569(9) to 2.007(9) Å in **1**, from 1.585(9) to 2.028(1) Å in **2**, from 1.584(9) to 2.015(8) Å in **3**, and from 1.582(6) to 2.003(5) Å in **4**. The As−O bond distances are in the range of 1.733(1)−1.806(8) Å in **1**, 1.733(1)−1.811(7) Å in **2**, 1.721(8)−1.805(8) Å in **3**, and 1.732(6)−1.803(5) Å in **4**. The valence sum calculations[20] show that the average empirical oxidation state valences of the V and As atoms are in 4.37 and 3.17 in **1**, 4.35 and 3.12 in **2**, 4.37 and 3.19 in **3**, and 4.33 and 3.16 in **4**, indicating that the oxidation state for each V atom and each As atom is +4 and +3, respectively. According to the electric charge of compound **4**, there is one H atom attached to the cluster, and the H atom could not be located by the crystal structure analysis. According to the related compounds reported previously, the H atoms attached to the polyoxoanion should be reasonable.[21]

(19) (a) Sheldrick, G. M. *SHELXS 97, Program for Crystal Structure Solution*; University of Göttingen: Göttingen, Germany, 1997. (b) Sheldrick, G. M. *SHELXL 97, Program for Crystal Structure Refinement*; University of Göttingen: Göttingen, Germany, 1997.

(20) Brown, I. D.; Altermatt, D. *Acta Crystallogr., Sect. B* **1985**, *41*, 244−247.

(21) (a) Honma, N.; Kusaka, K.; Ozeki, T. *Chem. Commun.* **2002**, 2896−2897. (b) Lin, B.; Chen, Y.; Liu, P. *Dalton Trans.* **2003**, 2474−2477.

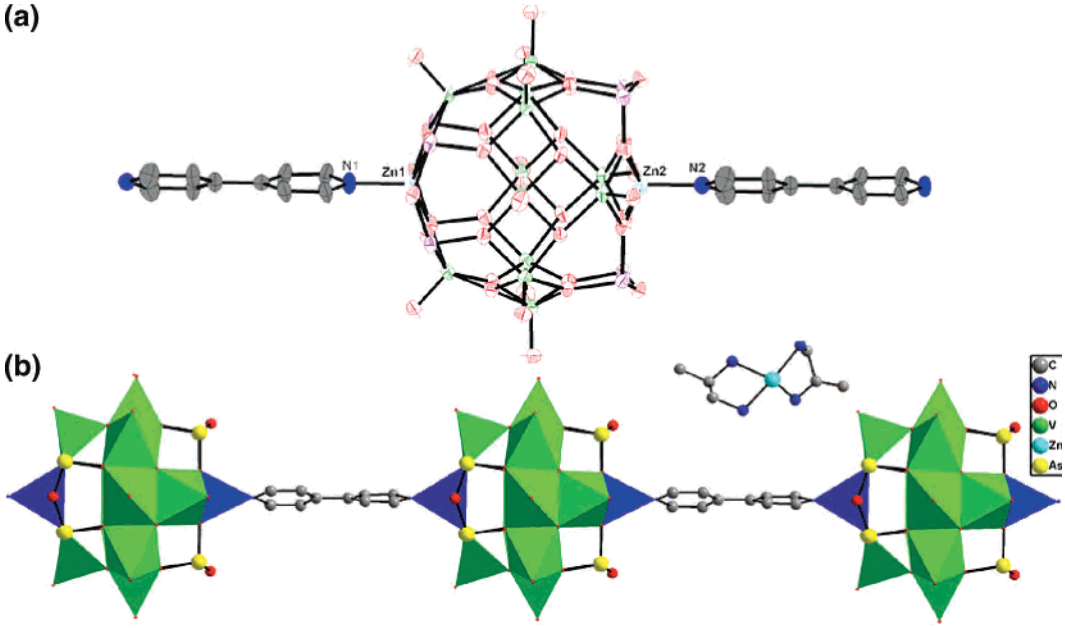

Figure 2. (a) ORTEP drawing of **1** with thermal ellipsoids at 30% probability. The guest molecules and H atoms have been omitted for clarity. (b) View of the 1D straight structure of **1**.

The structure of **1** consists of $\{(4,4'\text{-bipy})Zn_2As_8V_{14}O_{40}(H_2O)\}_n^{4n-}$ 1D chains and $[Zn(Meen)_3]^{2+}$ discrete countercations. Each $[Zn_2As_8V_{12}O_{40}]^{4-}$ cluster is directly linked to another two neighboring clusters by two 4,4′-bipy bridges, generating a 1D straight chain of $[-\{Zn_2As_8V_{12}O_{40}\}-4,4'\text{-bipy}-\{Zn_2As_8V_{12}O_{40}\}-]_\infty$ arrays (Figure 2). Each Zn atom on the backbone of the cluster bonds to one N donor from the 4,4′-bipy ligand [Zn1−N1 = 1.998(2) Å and Zn2−N2 = 1.949(2) Å] and four μ_3-O [Zn−O = 2.013(9)−2.039(8) Å] to furnish a square-pyramidal coordination environment. An interesting feature is that the TMC, $[Zn3(Meen)_2]^{2+}$, coexists in the crystal and occupies the interchain regions as a charge compensation. The Zn3 atom adopts tetrahedral geometry with Zn3−N bond lengths ranging from 2.002(0) to 2.105(1) Å. The $[(4,4'\text{-bipy})Zn_2As_8V_{14}O_{40}(H_2O)]_n^{4n-}$ chains are aligned to the *b* axis and pack each other along the *a* axis, generating a cluster anion layer along the *ab* plane, while the $[Zn(Meen)_3]^{2+}$ cations orderly reside between the layers as well as inside the channels to balance the negative charges of the clusters and to stabilize the structure of **1**.

In contrast to the straight-chain structure of compound **1**, **2** exhibits a 1D sinuate chain because of the effect of the TMC. The structure is constructed from $\{(4,4'\text{-bipy})Zn_2As_8V_{12}O_{40}\}_n^{4n-}$ 1D chains decorated with $[Zn(en)_2]^{2+}$ subunits through bridging O groups and electrically balanced by $[Zn(en)_2(H_2O)]^{2+}$ cations, shown in Figure 3. The $[Zn_2As_8V_{12}O_{40}]^{4-}$ cluster acts as a monodentate ligand supporting a $[Zn(3)(en)_2]^{2+}$ unit to give a new $[\{Zn(en)_2\}Zn_2As_8V_{12}O_{40}(H_2O)_{0.5}]^{2-}$ anion. Then each such anion cluster is further linked through two 4,4′-bipy bridges with two other neighboring clusters, generating a 1D sinuate chain of $[-\{\{Zn(en)_2\}Zn_2As_8V_{12}O_{40}\}-4,4'\text{-bipy}-\{\{Zn(en)_2\}Zn_2As_8V_{12}O_{40}\}-]_\infty$ arrays. Zn atoms adopt four different coordination environments in the asymmetric unit. The Zn1 and Zn2 atoms of the cluster are coordinated by four bridging O atoms [Zn1−O = 2.003(4)−2.064(1) Å; Zn2−O = 2.025(8)−2.051(8) Å] and one N atom from the 4,4′-bipy ligand [Zn1−N2 = 2.044(18) Å; Zn2−N1 = 2.041(26) Å] to complete the distorted square-pyramidal coordination environment. The Zn3 atom is coordinated by four N atoms from two en ligands [Zn3−N = 2.099(2)−2.199(2) Å] and one O atom from the V center of the $[Zn_2As_8V_{12}O_{40}]^{4-}$ anion with Zn3−O7 distances of 2.177(4) Å, exhibiting a $ONZnN_3$ trigonal bipyramid. The $OZn4N_4$ square pyramid is defined by four N donors of two en ligands and one O atom of coordinated water with a Zn4−O2W bond length of 2.023(3) Å and Zn4−N bond lengths of 2.101(2)−2.153(3) Å.

The adjacent 1D sinuate chains are stably packed together and exhibit an interesting 3D architecture via extensive hydrogen-bonding interactions among 4,4′-bipy groups, en ligands, water molecules, and polyoxoanions (Figure 4). The typical hydrogen bonds are C2···O15 = 3.327 Å, C10···O9 = 3.235 Å, OW1···OW6 = 2.609 Å, and OW6···O9 = 2.847 Å. It appears that the extensive hydrogen-bonding interactions play an important role in stabilizing the 3D supramolecular framework.

When the ratio of en and 4,4′-bipy ligands is changed moderately, the flexible en ligand is induced into the 1D chain of compound **3** and functionalized as the bridge ligand covalently bonding to the inorganic subunit. Single-crystal X-ray diffraction analysis reveals that two crystallographically independent $[Zn_2As_8V_{12}O_{40}]^{4-}$ clusters exist in the unit cell (Figure 5) of compound **3**. They first support $[Zn(en)_2]^{2+}$ complexes through N atoms from the en ligand in the form of $[Zn(cluster)enZn(en)_2]$ and further connect to each other to form an infinite 1D chain via en ligands and secondary metal complex bridges by the way of $-Zn(cluster1)enZn(en)_2O{=}V(cluster2)Zn(cluster2)enZn(en)_2O{=}V(cluster1)-$ in the *a* direction. By this means, the chain formed an eight-shaped helix, as shown in parts a and b of Figure 6. It is noteworthy that the two $[Zn_2As_8V_{12}O_{40}]^{4-}$ units are asymmetrically connected together via the secondary metal

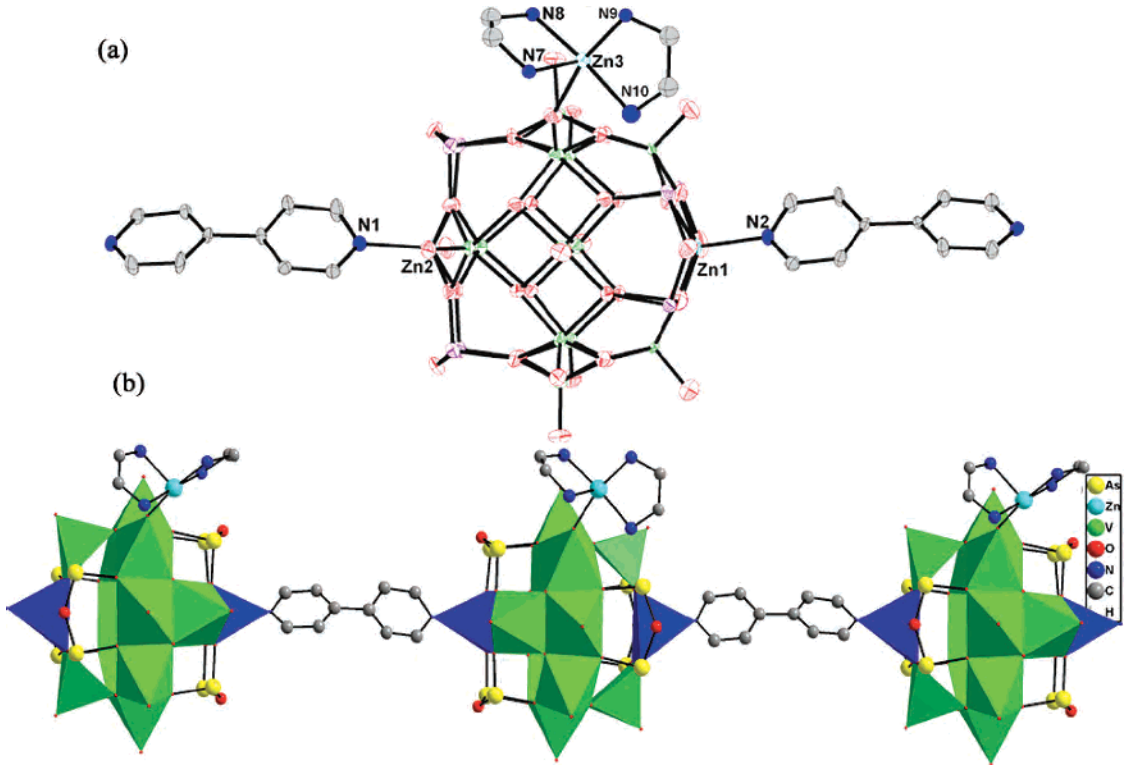

Figure 3. (a) ORTEP drawing of **2** with thermal ellipsoids at 30% probability. The guest molecules and H atoms have been omitted for clarity. (b) View of the 1D sinuate structure of **2**.

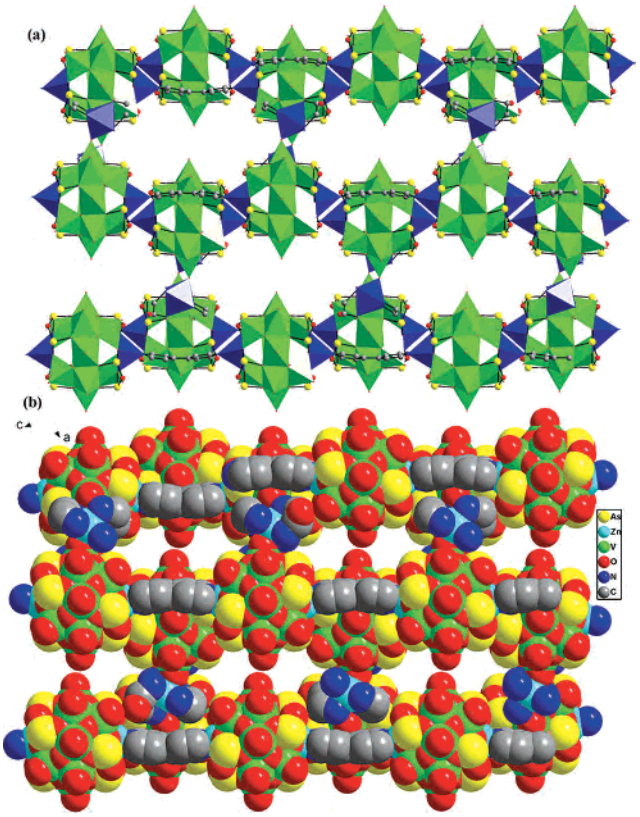

Figure 4. (a) Polyhedral and ball−stick representation of the 3D supramolecular structure of **2** along the *a* axis. (b) Space-filling diagram of the 3D supramolecular structure of **2**. The guest and isolated water molecules are omitted for clarity.

complexes and ligands to lead to the chirality in the whole chain structure. In order to well understand this structural feature, the eight-shaped helix is checked in detail. In each eight-shaped helix, two rings are very alike but different in bond atoms and bond lengths, that is, {O55−Zn7−N13−C13−C14−N14−Zn1−O4−V10−O16−V9} and {O15−Zn5−N3−C3−C4−N4−Zn4−O21−V11−O48−V6} heterocycles. Thus, we cannot find a symmetric center in the helical chain. However, compound **3** crystallizes in a centric space group $P2_1/n$, indicating that it is an equal mixture of right- and left-handed enantiomers. It is noteworthy that POMs with chiral or helical structures are of particular interest,[22] for instance, a chiral, nonracemizing, enantiomerically pure polyoxotungstate, $\{[\alpha\text{-}P_2W_{15}O_{55}(H_2O)]Zr_3(\mu_3\text{-}O)(H_2O)(L/D\text{-}tartH)[\alpha\text{-}P_2W_{15}O_{59}]\}$,[15−23] and a double-helical chain, $[(CH_3)_2NH_2]K_4[V_{10}O_{10}(H_2O)_2(OH)_4(PO_4)_7]\cdot 4H_2O$.[24] Compared with the other helical compounds, compound **3** presents the first eight-shaped helical, chiral chain consisting of TM-substituted POM building blocks.

In the structure of **3**, eight crystallographically distinct Zn sites display three different coordination environments: $NZn(1,2,3,4)O_4$ square pyramids, $N_2Zn(6,8)N_3$ trigonal bipyramids, and $ONZn(5,7)N_4$ distorted octahedra. The equatorial positions of the $NZnO_4$ square pyramid are occupied by four μ_3-O bridging atoms [Zn−O = 2.002(8)−2.076(9) Å], and the axial position is occupied by one N atom from an en ligand [Zn−N = 1.939(1)−2.026(1) Å]. Each distorted N_2-

(22) (a) Khan, M. I.; Chen, Q.; Salta, J.; O'Connor, C. J.; Zubieta, J. *Inorg. Chem.* **1996**, *35*, 1880−1901. (b) Zhang, L. J.; Zhou, Y. S.; Zuo, J. L.; Yu, Z.; Fun, H. K.; Abdul, I.; You, X. Z. *Inorg. Chem. Commun.* **2000**, *3*, 697−699.
(23) Fang, X. K.; Anderson, T. M.; Hill, C. L. *Angew. Chem., Int. Ed.* **2005**, *44*, 3540−3544.
(24) Soghomonian, V.; Chen, Q.; Haushalter, R. C.; Zubieta, J.; O'Connor, C. J. *Science* **1993**, *259*, 156−1599.

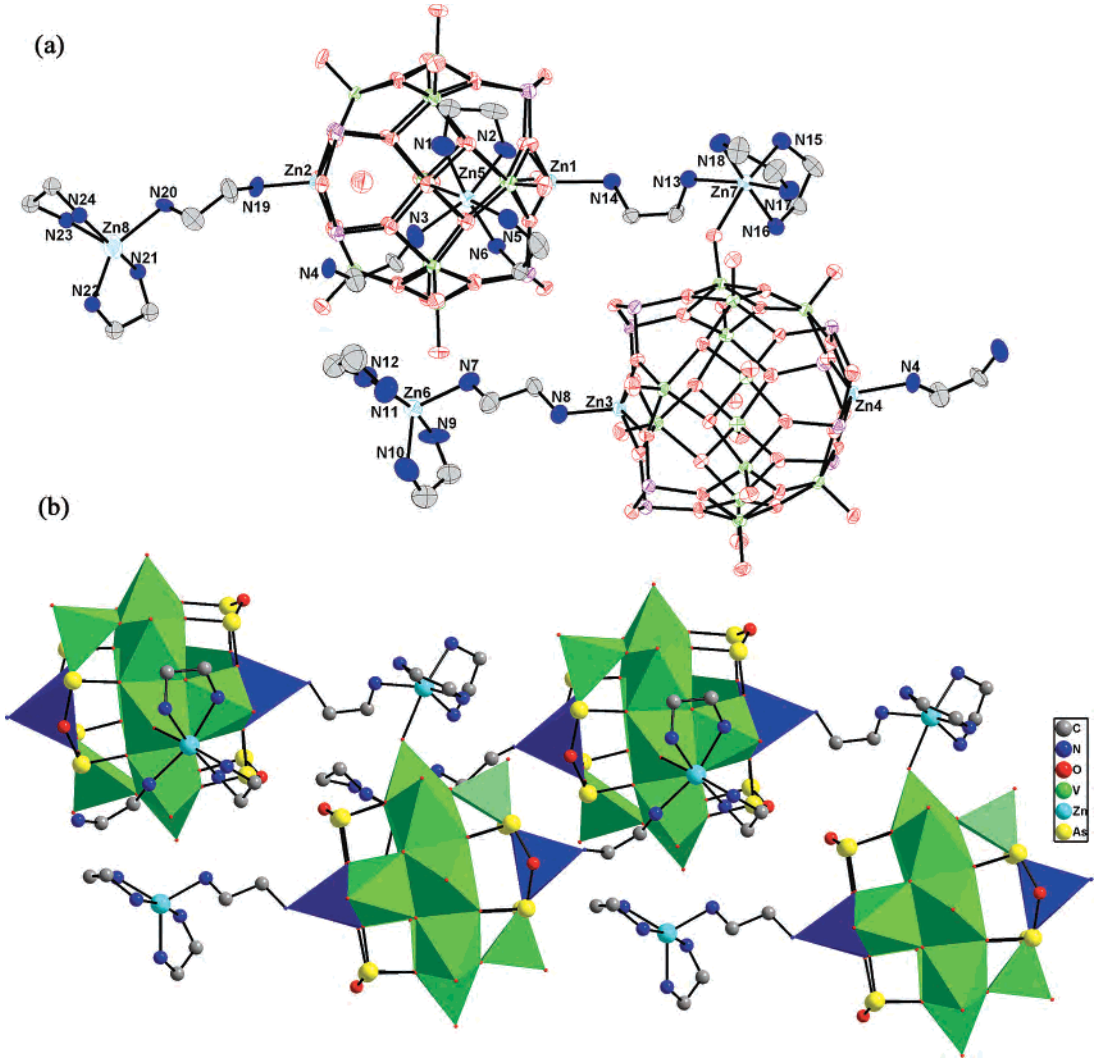

Figure 5. (a) ORTEP drawing of **3** with thermal ellipsoids at 30% probability. The guest molecules and H atoms have been omitted for clarity. (b) View of the 1D chain structure of **3**.

ZnN_3 trigonal bipyramid is defined by five N donors of two chelate en ligands and one bridging en ligand, respectively, with Zn−N bond lengths of 2.013(1)−2.160(2) Å. Each distorted octahedron $ONZnN_4$ is coordinated by five N atoms from two chelate en ligands and one bridging en ligand [Zn−N = 2.120(1)−2.196(1) Å] and one O atom from the $[Zn_2As_8V_{12}O_{40}]^{4-}$ anion with Zn5−O15 distances of 2.254(8) Å and Zn7−O55 distances of 2.263(8) Å. These unique coordination modes form three novel binuclear Zn cations (Figure 7a−c).

Another unusual feature of **3** is the coordination modes of en, shown in Figure 7. There are two coordination modes in the structure. Some act as common bidentate chelate ligands and coordinate to the Zn5, Zn6, Zn7, and Zn8 atoms to form $Zn(en)_2$ fragments. Others act as rare bridging ligands between the Zn centers (Zn1 and Zn4) of the Zn−As−V cluster and the $[Zn(5,7)(en)_2]^{2+}$-decorated Zn−As−V cluster or between the $[Zn(6,8)(en)_2]^{2+}$ fragment and the Zn centers (Zn2 and Zn3) of the Zn−As−V clusters in an end-to-end fashion. Notably, four types of configurations coexist in the structure. To the best of our knowledge, these different coordination modes and configurations of the en ligand coexisting in **3** have not been found in other POMs.

The 4,4′-bipy or en ligand associated with the Zn_2-substituted cluster building blocks from **1** to **3** limits structural expansion to higher dimensions. However, the presence of the secondary metal−ligand subunits decorating the surfaces of the clusters in **2** and **3** suggested a strategy for extension into two dimensions by tethering the secondary Zn complexes through bridging O groups of the POMs.

This expectation was realized with the isolation of **4**. Because of the large volume of the $[Zn_2As_8V_{12}O_{40}]^{4-}$ anion, the linking between chains may be difficult. We tried to use longer flexible, linear bpe instead of 4,4′-bipy to overcome this difficulty. As shown in Figure 8a,b, the 1D $\{(bpe)HZn_2As_8V_{14}O_{40}\}_n^{3n-}$ chains are linked through $[Zn(en)_2]^{2+}$ bridges to form a 2D network (Figure 8c,d). There are four crystallographically independent Zn atoms in an asymmetric unit. Each of the Zn sites (Zn3 and Zn4) located on the cluster exhibits square-pyramidal geometry with a N atom from the bpe ligand and four bridging O atoms [Zn3−N1 = 2.019(6) Å, Zn4−N2 = 2.021(7) Å, and Zn−O

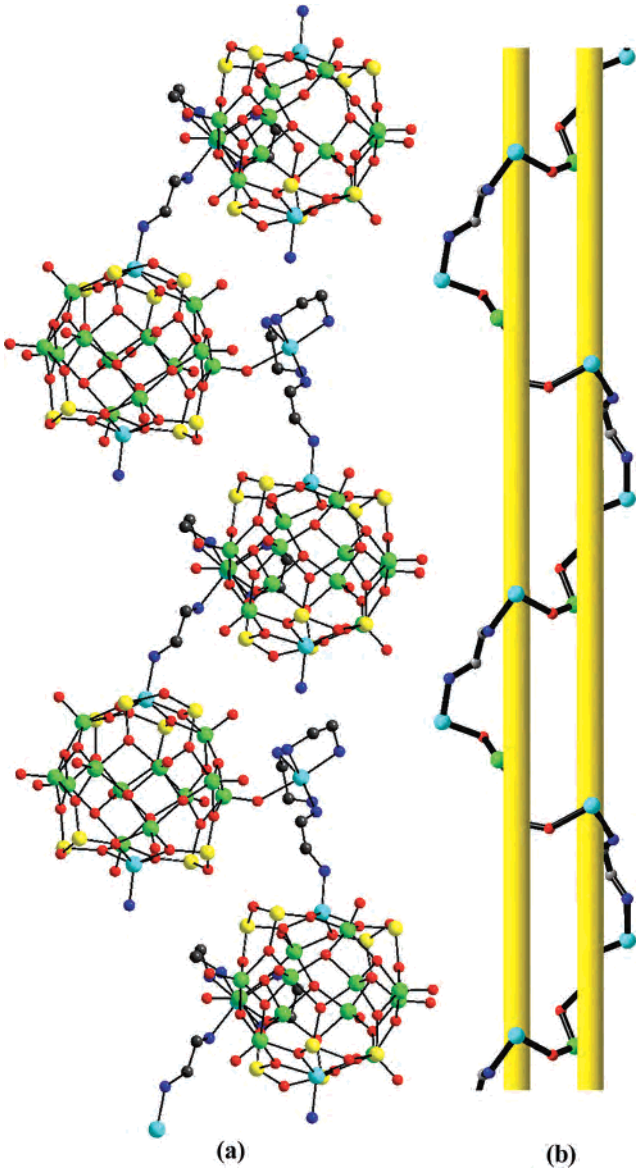

Figure 6. Ball−stick view of the eight-shaped helical chain of **3** (a) and a simple schematic presentation (b).

distances of 2.014(5)−2.061(6) Å]. Although the connection mode between $[HZn_2As_8V_{14}O_{40}]^{3-}$ and bpe of **4** is the same as those described in **1** and **2**, the arrangement of the parent clusters is quite different in **1** and **2** as a result of introducing the different ligands, bpe. It is notable that this kind of connectivity pattern results in the formation of a fascinating nanosized inner rectangular cavity of 33.669(6) × 14.720(8) Å, which is occupied by the lattice water molecules and guest $[Zn1_2(en)_5]^{4+}$ cations (Figure 8c,d). Worth mentioning here is that the $[Zn1_2(en)_5]^{4+}$ cation, which is a centrosymmetric ion, is still rare and the two Zn sites display the same coordination environment: a distorted ZnN_5 trigonal-bipyramidal configuration. Each Zn atom in binuclear TMC is coordinated by two en chelates and then linked up by an en bridge, as shown in Figure 7d. The distance of Zn1−N = 2.081(4)−2.156(2) Å is similar to those of the binuclear cation reported by Khan et al.[25] The interesting structural feature of **4**, however, is that the layers stack parallel to each other face to face in a staggered manner. $[Zn1_2(en)_5]^{4+}$ complexes are located in the rectangular cavities.

Another striking feature of compound **4** is the interesting arrangement of $[Zn(en)_2]^{2+}$, bpe, and $[HZn_2As_8V_{12}O_{40}]^{3-}$ clusters, which form a helical structure. In order to illustrate clearly, the left- and right-handed helical chains are represented, respectively, in Figure 9. Two $[HZn_2As_8V_{12}O_{40}]^{3-}$ clusters are first bridged by one bpe ligand, and then each pair of adjacent $[HZn_2As_8V_{12}O_{40}]^{3-}$ clusters is bridged by $[Zn(en)_2]^{2+}$ into a single-stranded helical chain running along the crystallographic 2_1 axis in the *b* direction with a long pitch of 22.591(5) Å. In addition, the adjacent helical chains in compound **4**, one exhibiting left-handed and the other right-handed helices, are bridged by bpe ligands to form a layer. As discussed above, the occurrence of a helical structure in compound **4** may be attributable to the fact that the steric orientation of the N groups is remarkably flexible. To our knowledge, compound **4** constitutes the first example of a 2D covalently bonded framework participated by organically modified Zn-substituted POMs, having both 1D large rectangular cavities and right- and left-handed helices.

Compared with all of the known structures of TM-substituted polyoxovanadates (Table 2), $[\{Zn(enMe)_2\}_2(enMe)_2\{Zn_2As_8V_{12}O_{40}(H_2O)\}]\cdot 4H_2O$[15] is a discrete Zn_2-substituted polyoxovanadate, $[Cd(dien)_2]_2[(dien)CdAs_8V_{13}O_{41}(H_2O)]\cdot 4H_2O$[26] is a discrete Cd-substituted polyoxovanadate, and $[Cd(en)_2]_2[(en)_2Cd_2As_8V_{12}O_{40}]$[26] and $\{[As_8V_{13}NiClO_{41}][Ni(en)_2(H_2O)][Ni(en)_2]\}\{[Ni(en)_2(H_2O)_2]_{0.5}\cdot 4H_2O$[27] are 1D chain-like polyoxovanadates linked by secondary metal complexes, while each Zn_2-substituted polyoxovanadate anion of compounds **1**−**4** is directly connected with adjacent anions through strong coordinated bonds by N-donor ligands to form 1D straight chains, sinuate chains, helical chiral chains, and finally a 2D layer. The secondary metal−ligand components function as countercations in **1**, supporting groups in **2** and **3**, and bridging groups in **3** and **4**. These compounds represent a new class of POM-based polymers with extended structure containing POM backbones coordinated directly by organic functionalities.

Synthesis. Compounds **1**−**4** were both separated from the hydrothermal reactions of NH_4VO_3, As_2O_3, $ZnCl_2\cdot 7H_2O$, HNO_3, and two kinds of N-donor ligands at 170 °C for 5 days. In a specific hydrothermal process, many factors can affect the formation and crystal growth of products, such as the initial reactants, starting concentrations, pH values, reaction time, and temperature. Each of these factors plays a significant role in the final structure. Because the reaction time and temperature were the same in this study, the other parameters could be examined more closely.

Organic Ligand Effects. Flexible and rigid N donors with different coordination abilities and geometries were chosen for this study, as shown in Chart 2. In the structures presented

(25) Khan, M. I.; Yohannes, E.; Doedens, R. J. *Inorg. Chem.* **2003**, *42*, 3125−3129.
(26) Zheng, S. T.; Zhang, J.; Xu, J. Q.; Yang, G. Y. *Inorg. Chem.* **2005**, *44*, 2426−2430.
(27) Cui, X. B.; Xu, J. Q.; Meng, H.; Zheng, S. T.; Yang, G. Y. *Inorg. Chem.* **2004**, *43*, 8005−8009.

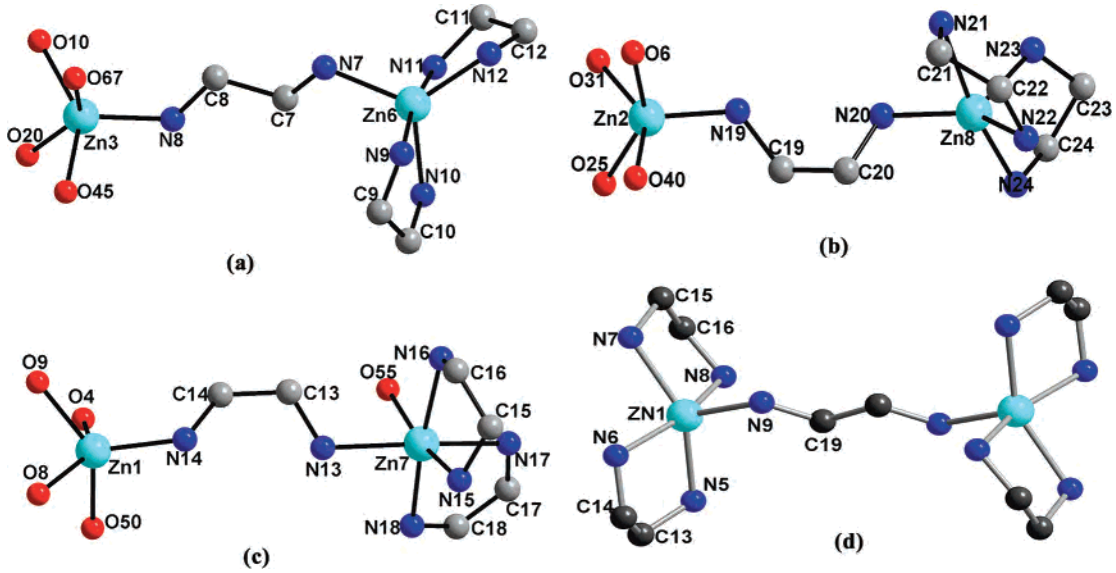

Figure 7. Interesting binuclear zinc organoamine complexes in **3** (a−c) and in **4** (d).

here, it is clear that the different linking manners and coordination preferences of the organic ligand have important influences on the construction of POM-based porous polymers. An organic ligand can not only directly coordinate to the backbone of $[Zn_2As_8V_{12}O_{40}]^{4-}$ to make the inorganic composition polymerized but also bind to secondary metal sites (TMCs) as an isolated charge-balancing cation, bridging groups, or supporting groups. For example, Meen ligands are observed to be in the chelating bidentate mode in **1**, bonding to zinc metal as a discrete charge-balancing cation. The en ligand was observed to be in the chelating bidentate mode, bonding to Zn atoms as a supported complex in **2** and **3** or as a bridging complex in **4**, and to be in the linear bridging mode, bonding between clusters via the substituted Zn atom as a supported zinc complex in **3** or forming the rare dimeric cation $[Zn_2(en)_5]^{4+}$ in **4**. All of the linear bipy ligands were functioning as bridging groups and directly covalently bonding to the Zn-substituted polyoxovanadates. We considered that the large volume of the cluster probably hinders the TMCs to link between the 1D chains of **2**. By manipulation of the spacer lengths and orientations of the pyridyl donors of the parent bipy and bpe ligands, the sinuate layers in **4** were successfully synthesized. The arrangement of clusters in the organic-functionalized POM main chains is quite different: the polyoxoanions are almost in a line in **1** and **2** for the rigid ligand, while in **3** and **4**, the clusters are staggered for the flexible ligand.

Secondary Metal. The Zn source of the reaction system was of crucial importance for the crystallization of products **1**−**4**. The black crystals of compounds **1**−**4** could be obtained only using $ZnCl_2 \cdot 7H_2O$. We have tried to replace $ZnCl_2 \cdot 7H_2O$ with other transition metals, but no isostructural compounds of **1**−**4** were obtained, except one compound $[Cd(en)_2]_2[(en)_2Cd_2As_8V_{12}O_{40}(H_2O)] \cdot nH_2O$ formed when $CdCl_2 \cdot 0.5H_2O$ was added into the reaction system. There could be two reasons for this: (1) the spherical d^{10} configuration is associated with a flexible coordination environment so that the geometries of the Zn atom can vary from tetrahedron through trigonal bipyramid and square pyramid to octahedron and severe distortion of the ideal polyhedron easily occurs. Consequently, Zn can readily accommodate the forms of different architectures. In the present case, the Zn atom adopts a square-pyramidal coordination geometry to replace the V atom with similar coordination geometry on the inorganic cluster and/or tetrahedron, trigonal bipyramid, and octahedron to bind to organic ligands as the secondary metal center (Table 2). However, other transition-metal atoms, such as Mn, Fe, Co, and Ni are hardly involved. (2) The type of metal salt in the reaction mixture may affect the formation of compounds **1**−**4**. Because the Zn^{2+} and Cl^- ions of $ZnCl_2 \cdot 7H_2O$ can be dispatched thoroughly in the low-concentration aqua, Zn^{2+} easily takes part in the cluster architectures. In the parallel experiments, $ZnCl_2 \cdot 7H_2O$ was replaced by $Zn(MeCO_2)_2 \cdot 2H_2O$, $Zn(NO_3)_2 \cdot 2H_2O$, or $ZnSO_4$, but only green slurry and amorphous solids could be obtained.

Furthermore, the direct replacement of the VO^{2+} group by a Zn atom results in an activity position for covalent attachment to an organic ligand, which provides a possible manipulation of the structures and properties by inducing various organic ligands.

pH Value. The pH value of the reaction system is a key factor for the formation of POMs. In comparison with other POMs, the formation environment of these substituted As−V−O clusters was in a more basic solution than the environment in the syntheses of As−V−O clusters. Compounds **1**−**4** were synthesized at approximately pH 8−10. If the reaction solution is below 7, there will not be a crystalline phase, and the products were a mixture of green powder. The higher basic environment is more beneficial to the deprotonation of N ligands, consequently bonding to the metal Zn ions easily in this work.

FT-IR Spectroscopy. The IR spectra of all of the compounds have characteristic υ(V═O), υ(V−O−M), and υ(As−O) (M = V, Zn, or As) asymmetric stretching vibration peaks at 987, 827, 718, 638, 548, and 460 cm^{-1}

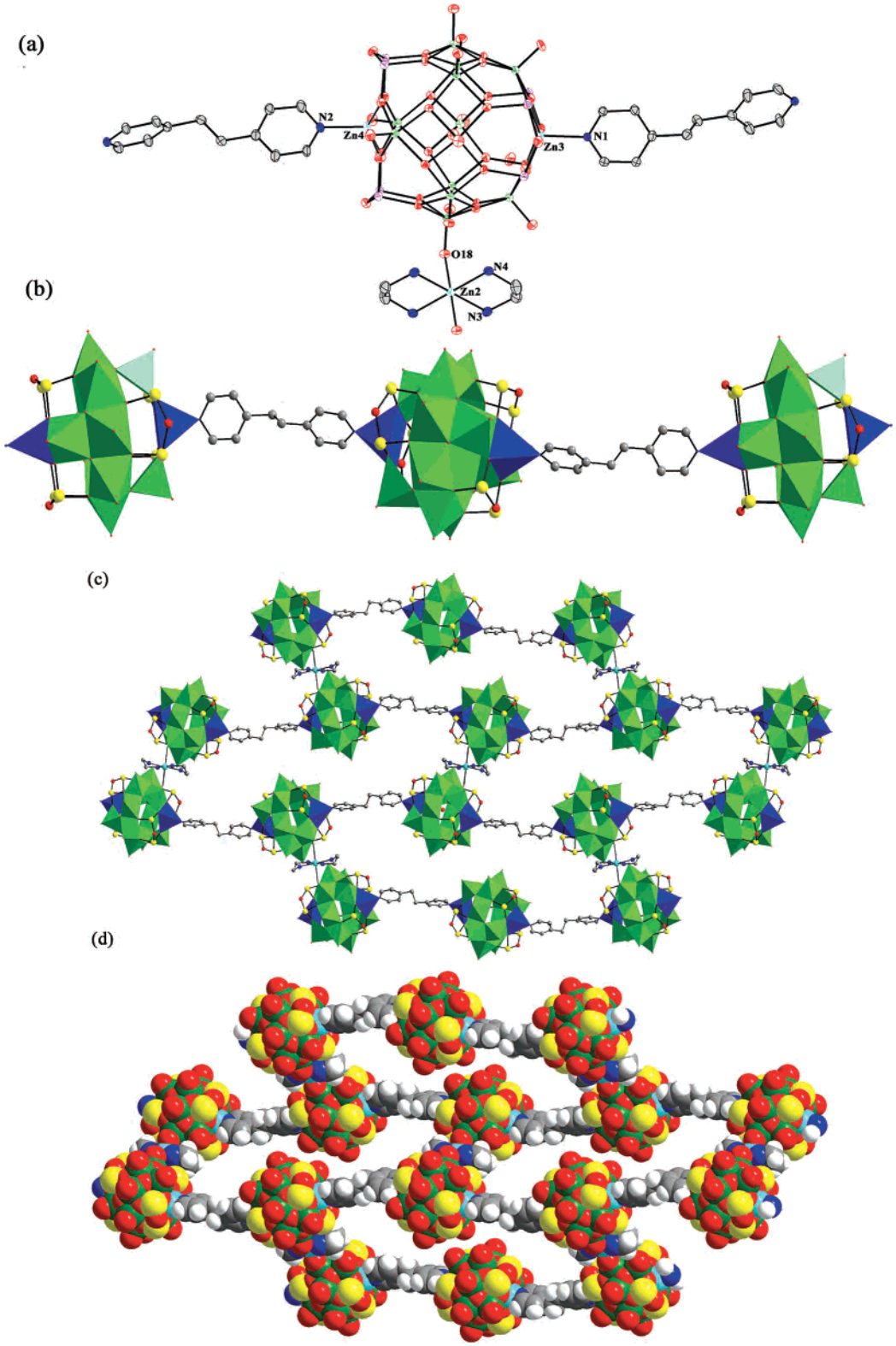

Figure 8. (a) ORTEP drawing of **4** with thermal ellipsoids at 30% probability. The guest molecules and H atoms have been omitted for clarity. (b) View of the sinuate chain of $[HZn_2As_8V_{12}O_{40}]$ linked by bpe ligands. (c) View of $[(bpe)HZn_2As_8V_{12}O_{40}]$ chains linked by $[Zn(en)_2]^{2+}$ to a layer with a rectangular cavity. (d) Space-filling diagram of the open-framework motif. The guest, $\{[Zn(en)_2]_2(en)\}^{2+}$, and isolated water molecules are omitted for clarity.

for **1**, at 987, 822, 711, 631, 545, and 455 cm^{-1} for **2**, at 982, 817, 716, 636, 547, and 460 cm^{-1} for **3**, and at 984, 824, 715, 639, 544, and 465 cm^{-1} for **4**, as shown in Figures S4−S7 in the Supporting Information, suggesting that the substituted polyoxoanion moiety $[Zn_2As_8V_{14}O_{40}]^{4-}$ in the complexes **1**−**4** still remains the backbone of the parent $[As_8V_{14}O_{42}]^{4-}$ cluster. However, perturbed by organic groups, the stretching vibrational bands υ(V−O−M) and υ(As−O) have red shift. The characteristic absorption bands of organoamine ligands occur at 3251, 2961,1608, 1460, 1420,

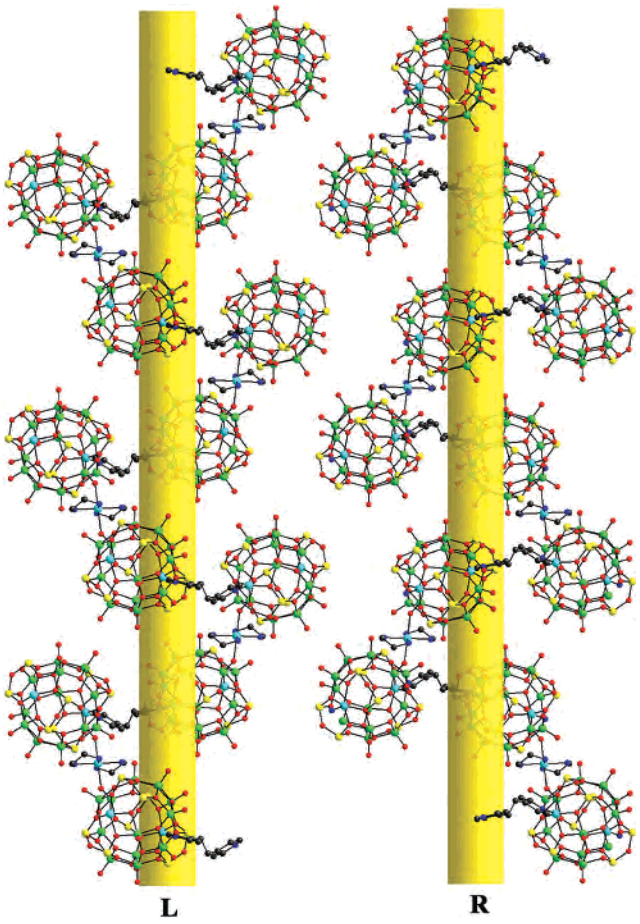

Figure 9. View of the right- and left-handed helices in **4**.

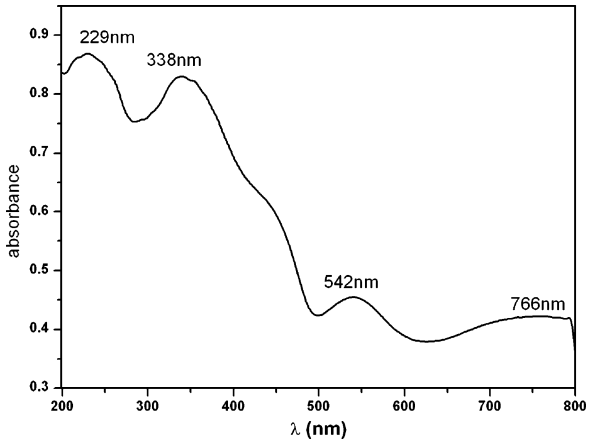

Figure 10. UV−vis absorption spectrum of **4**.

1303, 227, and 1075 cm^{-1} for **1**, at 3269, 2931, 1606, 1530, 1496, 1460, 1420, 1332, 1279 1221, and 1098 cm^{-1} for **2**, at 3269, 2942, 1591, 1459, 1412, 1284, and 1104 cm^{-1} for **3**, and at 3265, 2944, 1616, 1505, 1460, 1369, 1244, and 1074 cm^{-1} for **4**.

UV−Vis Spectrum. The UV−vis spectrum of compound **4** in solid form shows intense absorption bands in the range from 200 to 600 nm with three main shoulders at ca. 229, 338, and 542 nm (Figure 10), corresponding to oxide-to-vanadium charge-transfer transitions.[28] In the visible region, the broad band appearing in at 766 nm is assigned as an intervalence charge-transfer band, $V^{IV}-V^{V}$.

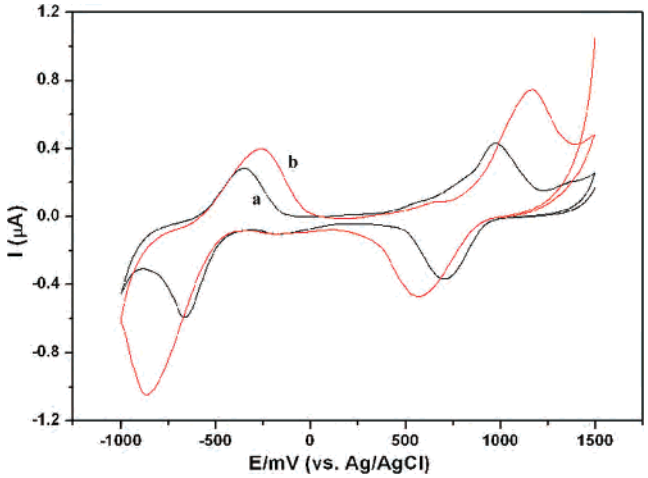

Figure 11. Comparative cyclic voltammograms of **1**−CPE in 1 M H_2SO_4 (a) and a 50% (v/v) ethanol + 1 M H_2SO_4 medium (b). Potentials vs SCE. Scan rate: 50 mV s^{-1}.

TGA. The TGA were carried out in flowing N_2 with a heating rate of 10 °C min^{-1} in the temperature range 25−700 °C for compounds **1**−**4**, as shown in Figures S8−S11 in the Supporting Information. All of the weight losses of the four complexes are attributable to the loss of water molecules, the decomposition of organoamine ligands, and the sublimation of As_2O_3. In the curve of compound **1**, the first weight loss in the range of 25−148 °C corresponds to the loss of water molecules; the last three continuous weight losses at 224−800 °C can be attributed to the decomposition of organoamine ligands and the sublimation of As_2O_3. The whole weight loss 47.95% is in agreement with the calculated value 47.01%. The sample does not lose weight at temperatures higher than 800 °C. Three continuous weight losses were found at 25−736 °C in compound **2**. The whole weight loss 48.58% is in agreement with the calculated value 49.18%. Similarly three continuous weight-loss curves are observed on the TGA curve of compound **3**. The observed whole weight loss (48.89%) between 25 and 729 °C is consistent with the calculated value (49.24%). Two weight losses were found in the TGA curve of compound **4**, which occur at 43−461 and 461−535 °C. The observed weight loss (47.19%) is consistent with the calculated value (48.07%). All of the remaining products in compounds **1**−**4** are a mixture of ZnO and VO_2.

Electrochemical Property. POMs have attracted much interest in electrode modification and electrocatalysis fields because of their ability to undergo a series of reversible multielectron redox processes. Especially, vanadium oxides are of particular interest as candidates for active cathode materials in reversible lithium batteries or electrochemical devices; the electrochemical activities of **1**−**4** were investigated. To determine the redox properties of compounds **1**−**4**, bulk-modified CPE was fabricated as the working electrode because of its insolubility in most solvents.[29,30] Chemically, bulk-modified CPE is a mixture of a modifier, graphite powder, and pasting liquid and has been widely

(28) Chen, Q.; Goshorn, D. P.; Scholes, C. P.; Tan, X. L.; Zubieta, J. *J. Am. Chem. Soc.* **1992**, *114*, 4667−4681.

Table 2. Comparison of Selected Structural Characteristics of TM-Substituted Polyoxovanadates

compound	organic ligand	overall dimensionality	hybrid metal building block	ref
1	Meen, 4,4′-bipy	1D straight chain	$NZnO_4$ square pyramid: substituted and bridge group ZnN_4 tetrahedron: countercations	this work
2	en, 4,4′-bipy	1D sinuate chain	$NZnO_4$ square pyramid: substituted and bridge group $ONZnN_3$ trigonal bipyramid: support group $OZnN_4$ square pyramid: countercations	this work
3	en, 4,4′-bipy	1D helical chiral chain	$NZnO_4$ square pyramid: substituted and bridge group $ONZnN_4$ octahedron: bridge group N_2ZnN_3 trigonal bipyramid: support group	this work
4	en, bpe	2D layer with helix	$NZnO_4$ square pyramid: substituted and bridge group O_2ZnN_4 octahedron: bridge group N_2ZnN_3 trigonal bipyramid: binuclear countercations	this work
$[\{Zn(enMe)_2\}_2(enMe)_2\{Zn_2\text{-}As_8V_{12}O_{40}(H_2O)\}]\cdot 4H_2O$	Meen	isolated cluster	NZnO square pyramid: substituted group N_2ZnN_3 trigonal bipyramid: support group	16
$[Cd(dien)_2]_2[(dien)CdAs_8V_{13}O_{41}(H_2O)]\cdot 4H_2O$	dien	isolated cluster	N_3CdO_4 decahedron: substituted group	26
$[Cd(en)_2]_2[(en)_2Cd_2As_8V_{12}O_{40}]$	en	1D straight chain	O_4CdN_2 octahedron: substituted group O_2CdN_4 octahedron: bridge group	26
$\{[As_8V_{13}NiClO_{41}][Ni(en)_2(H_2O)][Ni(en)_2]\}\{[Ni(en)_2(H2O)_2]_{0.5}\cdot 4H_2O$	en	1D straight chain	$ClONiO_4$ octahedron: substituted group O_2NiN_4 octahedron: bridge group	27

Chart 2. Coordination Modes of the Various Ligands in Compounds **1**−**4**

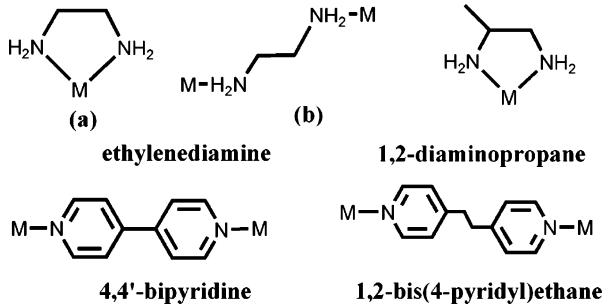

applied in electrochemistry owing to its many advantages: it is inexpensive, easy to handle, and easy to prepare. Because of similar basic building blocks in **1**−**4**, the redox peaks of compounds **1**−**4** are expected to behave similarly. We carefully studied the redox property of compound **1** and other compounds in brief. In short, four issues were found to be pertinent for this electrochemical study: (1) the redox behaviors of compounds **1**−**4**; (2) the effect of complex fragments and ligands; (3) the media effects on **1**−CPE; (4) the electrocatalytic activity of **1**−CPE.

Voltammetric Behavior of Compounds−CPE. The voltammetric behaviors of the working electrodes at different scan rates in 1 M H_2SO_4 aqueous solutions are shown in Figure S12 in the Supporting Information. The four compounds exhibit similar electrochemical behaviors except some displacements. It can be seen that, in the potential range +1150 to −1000 mV at a scan rate of 50 mV s^{-1}, two quasi-reversible redox peaks appear and the mean peak potentials $E_{1/2} = (E_{pa} + E_{pc})/2$ are +837 (I) and −508 (II) mV in compound **1**, +864 (I) and −517 (II) mV in compound **2**, +854 (I) and −508 (II) mV in compound **3**, and +862 (I) and +551 (II) mV in compound **4**, respectively. The redox peaks I−I′ and II−II′ may be attributable to V^V/V^{IV} and V^{III}/V^{IV}, respectively. Compared with a previously reported process,[31] both the cathodic peak potentials and the corresponding anodic peak potentials shifted to the positive direction. When the scan rate varied from slow to fast, the peak potentials in compounds **1**−**4** changed gradually: the cathodic peak potentials shifted to the negative direction and the corresponding anodic peak potentials shifted to the positive direction with increasing scan rate. It should be pointed out that the peak-to-peak separation between the corresponding cathodic and anodic peaks increases with increasing scan rate.[32]

Influence of the Complex Fragments. The peak potentials of the two pairs of redox peaks are hardly displaced, irrespective of whether the complex fragment is $[Zn(Meen)_3]^{2+}$, $[Zn(en)_2]^{2+}$, or $[Zn_2(en)_5]^{4+}$ and the organic ligand is 4,4′-bipy or bpe. The values of $E_{1/2}$ among compounds **1**−**4** are close. The small difference in $E_{1/2}$ among compounds **1**−**4** suggests that core $[Zn_2As_8V_{12}O_{40}]^{4-}$ is the active center for the electrochemical redox activity in CPE, while the corresponding complex fragments have only a slight effect on the electrochemical behavior of **1**−, **2**−, **3**−, or **4**−CPE.

Voltammetric Behavior of 1−CPE in a Mixed-Solvent Electrolyte. Wang and Dong have reported the media (50% water + ethanol medium containing H_2SO_4) effects on the redox properties of $PMo_{12}O_{40}^{3-}$ and $SiMo_{12}O_{40}^{4-}$ film modified carbon fiber microelectrodes.[33] In the present study, we also investigated media effects on the redox properties of **1**−CPE in the polar solvent (ethanol), and the percentage of organic solvent in the electrolyte was kept at 50% by volume. Figure 11 shows comparative cyclic voltammograms of **1**−CPE in 1 M H_2SO_4 (a) and 50% (v/v) ethanol + 1 M

(29) Duan, L. Y.; Liu, F. C.; Wang, X. L.; Wang, E. B.; Qin, C. *J. Mol. Struct.* **2004**, *705*, 15−20.
(30) Wang, X. L.; Wang, E. B.; Lan, Y.; Hu, C. W. *Electroanalysis* **2002**, *14*, 1116−1121.
(31) Gorski, W.; Cox, J. A. *Langmuir* **1996**, *11*, 3603−3604.
(32) Pope, M. T.; Papaconstantinou, E. *Inorg. Chem.* **1967**, *6*, 1147−1152.
(33) Wang, B.; Dong, S. *Electrochim. Acta* **1996**, *41*, 895−902.

H_2SO_4 (b) media at 50 mV s^{-1}. It can be clearly seen that in the ethanol−H_2SO_4 mixed solvent all of the cathodic peak potentials (E_p) of the two redox waves shift to the negative potential direction and the peak-to-peak separations between the corresponding cathodic and anodic peaks increase, especially when the scan rate is increased. In an aqueous acidic solution, some of the protons that diffused into POM are attached to the O_b atoms of the $[Zn_2As_8V_{12}O_{40}]^{4-}$ cluster by bonding, and this easily results in a redox reaction in the presence of protons on the CPE, while other protons may adsorb around compound **1** as a result of some other effect. However, in the presence of ethanol molecules, these organic solvent molecules may also be adsorbed around compound **1**, and this adsorption effect is stronger than that of the protons, which hinders the diffusion of the protons and thus decreases the electron-exchange rate between compound **1** and the electrode surface.

Electrocatalytic Activity of 1−CPE. As is known, POMs are capable of delivering electrons to other species, thus serving as powerful electron reservoirs for multielectron reductions. This property has been exploited extensively in electrocatalytic reductions. For example, Dong et al. observed that $SiW_{12}O_{40}^{4-}$ could be used as an electrocatalyst for the reduction of nitrite.[34] Generally, an inorganic or organic electrocatalyst exhibits a single electroreductive or electrooxidative catalytic activity. It has been a challenge to develop a bifunctional electrocatalyst, particularly a system that can catalyze both oxidation and reduction. Furthermore, the electrocatalytic properties of V-containing POMs have drawn attention only in recent years, and the electrochemical properties of the full-reduction type of polyoxovanadates have rarely been reported. In our experiment, we found that **1**−CPE, a full-reduction V^{IV}-containing POM, presents electrocatalytic activity toward the reduction and oxidation of hydrogen peroxide and nitrite.

Parts A and B of Figure 12 show cyclic voltammograms for the electrocatalytic reduction of hydrogen peroxide and nitrite at a bare CPE and at **1**−CPE in a 1 M H_2SO_4 aqueous solution. No obvious voltammetric response is observed in the potential range from −1000 to +1500 mV for hydrogen peroxide and nitrite at a bare CPE. At **1**−CPE, with the addition of hydrogen peroxide and nitrite, the II′ reduction peak current increases gradually while the corresponding II oxidation peak current gradually decreases. On the contrary, the I oxidation peak current increases while the corresponding I′ reduction peak decreases, which suggests that hydrogen peroxide and nitrite are reduced by reduced species of the II−II′ processes and oxidized by the I−I′ processes. Therefore, **1**−CPE can be considered as a kind of potential bifunctional electrocatalyst that both oxidation and reduction functions toward hydrogen peroxide and nitrite by adjusting the potential range.

Magnetic Property. The variable-temperature magnetic susceptibilities of compounds **1** and **4** were measured from 2 to 300 K at 1 T and are shown in Figures 13 and S13 (in the Supporting Information), exhibiting quite similar mag-

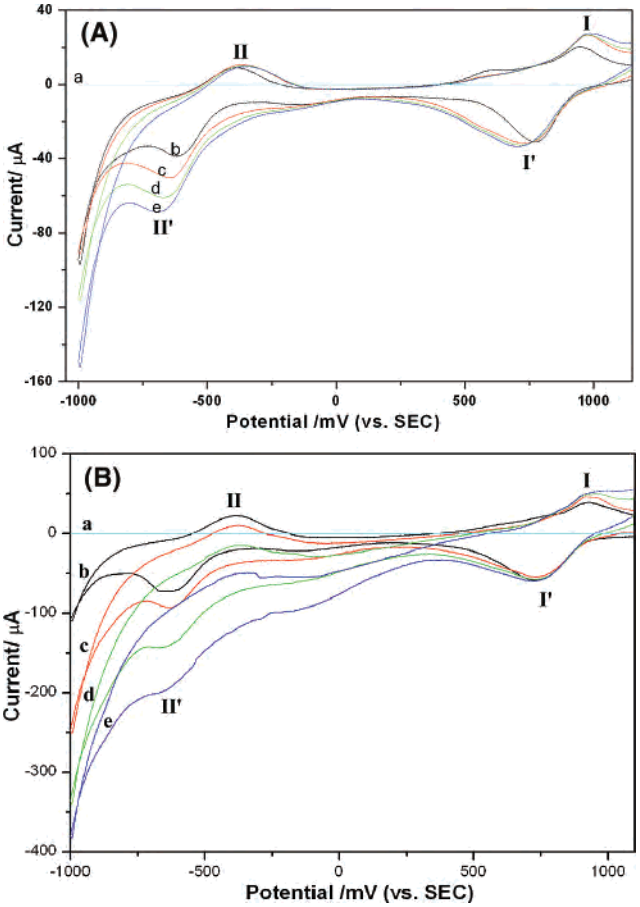

Figure 12. (A) Cyclic voltammograms of a bare CPE in a 20 mM H_2O_2 + 1 M H_2SO_4 solution (a). **1**−CPE in a 1 M H_2SO_4 solution containing 0 (b), 5 (c), 15 (d), and 25 (e) mM H_2O_2. Potentials vs SCE. Scan rate: 50 mV s^{-1}. (B) Cyclic voltammograms of a bare CPE in a 20 mM $NaNO_2$ + 1 M H_2SO_4 solution (a). **1**−CPE in a 1 M H_2SO_4 solution containing 0 (b), 10 (c), 20 (d), and 30 (e) mM $NaNO_2$. Potentials vs SCE. Scan rate: 50 mV s^{-1}.

netic behavior. In compound **1**, as T is reduced, the $\chi_M T$ value continuously decreases nearly linearly to 0.97 cm^3 K mol^{-1} at 45 K and then decreases rapidly from 45 K, reaching a minimum value of 0.32 cm^3 K mol^{-1} at 2 K. Such magnetic behavior is characteristic of an antiferromagnetic coupling interaction. $\chi_M T$ shows a value of 1.16 cm^3 K mol^{-1} at room temperature, which is much lower than the expected value (4.5 cm^3 K mol^{-1}) for 12 uncoupled $S = {}^1/_2$ spins of V^{4+} atoms (assuming $g = 2$ for V^{4+}). Similar trends have also been observed in $[\{Zn(enMe)_2\}_2(enMe)_2\{Zn_2As_8V_{12}O_{40}(H_2O)\}]\cdot 4H_2O$ and other high-nuclearity-spin oxovanadium clusters.[35−37] These antiferromagnetic coupling interactions are related to electron delocalization. Previous studies indicated that electron delocalization could favor spin pairing. In compound **1**, the short neighboring V···V distances of V1···V5 (2.921 Å) and V3···V6 (2.855 Å) and their equatorial site pairs with O bridges lie in the range expected for strong antiferromagnetic coupling, thus resulting in a low

(34) Dong, S.; Xi, X.; Tian, M. *J. Electroanal. Chem.* **1995**, *385*, 227.

(35) Gatteschi, D.; Pardi, L.; Barrar, A. L.; Müller, A.; Döring, J. *Nature* **1991**, *354*, 463−465.

(36) Gatteschi, D.; Pardi, L.; Barrar, A. L.; Müller, A.; Döring, J. *J. Am. Chem. Soc.* **1992**, *114*, 8509−8514.

(37) Yamase, T.; Makino, H.; Naruke, H.; Wéry, A. M. S. J. *Chem. Lett.* **2000**, *12*, 1350−1351.

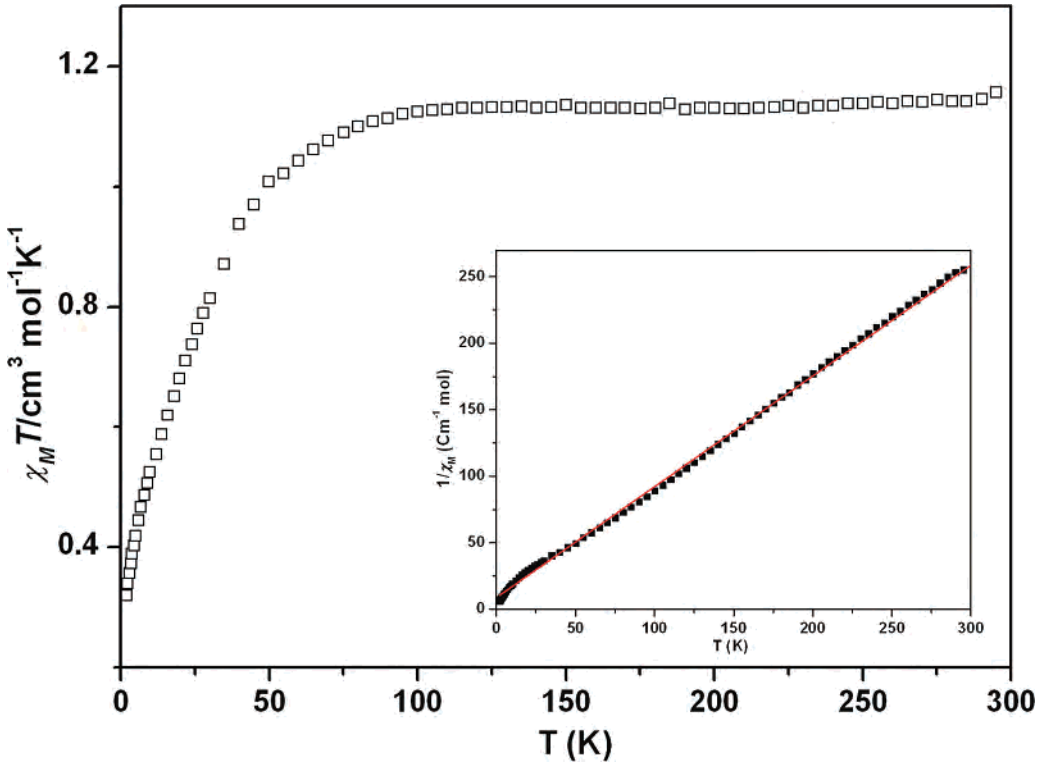

Figure 13. Plot of $\chi_M T$ vs T for **1**.

$\chi_M T$ value at high temperature. The remaining four V ions (V2 and V4 and their equatorial sites) are largely uncorrelated at high temperature. The magnetic susceptibility obeys the Curie−Weiss law in the whole range of 40.0−300.0 K, giving a Weiss constant $\theta = -10.31$ K and a Curie constant $C = 1.2$ cm^3 K mol^{-1}, characteristic of an overall antiferromagnetic interaction.

Because the Zn organic chains did not pay any paramagnetic contribution, the $\chi_M T$ products of compounds **1** and **4** are almost dependent upon the polyoxovanadate anions, which are quite similar to those related isolated complexes.[16,26] A more detailed magnetic discussion of **1** and **4** is still underway.

Conclusions

The novel system of solids $[Zn(Meen)_2]_2[(4,4'\text{-bipy})Zn_2As_8V_{12}O_{40}(H_2O)]$ (**1**), $[Zn(en)_2(H_2O)][Zn(en)_2(4,4'\text{-bipy})Zn_2As_8V_{12}O_{40}(H_2O)]\cdot 3H_2O$ (**2**), $[\{Zn(en)_3\}_2\{Zn_2As_8V_{12}O_{40}(H_2O)\}]\cdot 4H_2O\cdot 0.25$bipy (**3**), and $[Zn_2(en)_5]\{[Zn(en)_2][(bpe)HZn_2As_8V_{12}O_{40}(H_2O)]_2\}\cdot 7H_2O$ (**4**) is successfully prepared by the idea of incorporating organic-functionalized POM and secondary metal complex strategies. This approach is complementary to the covalent polymers of POMs and secondary metal complex decorated POMs reported in the literature. This work also demonstrates that the rigid/flexible ligands have a crucial influence on the formation of products. If the ligands were properly controlled, inorganic oxide units and organic ligands could "work" together very well to produce interesting compounds with distinctive frameworks. On the other hand, the functional Zn_2-substituted polyoxovanadate cluster $[Zn_2As_8V_{12}O_{40}]^{4-}$ exhibits interesting coordination features of constructing an extended structure through direct covalent bonding to N-donor ligands. Furthermore, different coordination environments of the secondary metal and the pH value play important roles in the structures of the products. Generally, this work extends the known organic−inorganic hybrid materials. It is certainly optimistic that the combination of the inorganic TM-substituted POMs, second metal, and mixed flexible and/or rigid ligands may provide a chance for realization of material design and the preparation of more favorable models for material science.

Acknowledgment. This work was financially supported by the National Science Foundation of China (Grant 20371011).

Supporting Information Available: X-ray crystallographic files for **1**−**4** in CIF format, additional figures, IR spectra, and TGA curves. This material is available free of charge via the Internet at http://pubs.acs.org.

IC062338L